Electron density effects in the modulation spectroscopy of strained and lattice-matched InGaAs/InAlAs/InP high-electron-mobility transistor structures

A. Dimoulas,[a] J. Davidow, and K. P. Giapis
Division of Chemistry and Chemical Engineering, California Institute of Technology, 210-41, Pasadena, California 91125

A. Georgakilas, G. Halkias, and N. Kornelios
Foundation for Research and Technology-Hellas, P. O. Box 1527, Heraklion 711 10, Greece

(Received 12 February 1996; accepted for publication 4 June 1996)

The effects of the channel electron density on the interband optical transitions of strained ($x=0.6$ and 0.65) and lattice-matched ($x=0.53$) $In_xGa_{1-x}As/In_{0.52}Al_{0.48}As/InP$ high-electron-mobility transistor structures have been investigated by phototransmittance at room temperature. Analysis of the ground and first excited transitions for low and high densities, respectively, enabled a separate estimation of the electron densities occupying each one of the first two subbands. It was found necessary to include the modulation of the phase-space filling in the analysis of the spectra, especially for the samples with a high electron density, in which case this modulation mechanism becomes dominant. © *1996 American Institute of Physics.* [S0021-8979(96)01418-1]

I. INTRODUCTION

Modulation spectroscopy (MS), and especially its contactless version photoreflectance (phototransmittance), can effectively characterize epitaxial semiconductor multilayers[1] at room temperature. In *n*-type modulation-doped quantum-well heterostructures and high-electron-mobility transistors (HEMTs), the electron density n_s in the active channel is an important parameter determining their high-power performance characteristics. The possibility of estimating n_s by using MS has been the subject of a considerable dispute during the past 10 years.[1] In GaAs/AlGaAs modulation-doped field-effect transistors (MODFETs), the presence of a large signal from the GaAs buffer layer renders the analysis of the spectra difficult and inconclusive.[1] Our understanding of the electron density effects on the optical transitions has been substantially improved by studying the pseudomorphic AlGaAs/InGaAs/GaAs HEMT structure,[2–5] where the signals from the GaAs buffer and the two-dimensional electron gas in the active InGaAs channel are spectrally separated (by about 0.15 eV). While a theoretical analysis based on first principles is already available,[6] the dominant modulation mechanism remains an unresolved question.[2–5,7,8] A more thorough investigation must consider alternative heterostructures, for example, the $In_xGa_{1-x}As/In_{0.52}Al_{0.48}As/InP$ HEMTs, in order to ensure that the experimental and theoretical results are generally valid. The latter heterostructure offers the advantage of well-resolved phototransmittance signals in the InGaAs channel, with a negligible influence from the InP absorption edge due to a large (more than 0.6 eV) spectral separation. With the exception of differential absorption spectroscopy measurements on only one lattice-matched sample,[9] no modulation spectroscopy results have been reported, despite the fact that the InGaAs/InAlAs/InP HEMT is a technologically important device known to perform at frequencies in excess of 100 GHz with low noise.[10]

In the present work, several strained ($x=0.6$ and 0.65) and lattice-matched ($x=0.53$) HEMTs with different channel widths and electron densities are investigated by phototransmittance at room temperature. The merits and limitations of using MS for a complete characterization of HEMTs with respect to electron density are discussed. By including the derivative of the absorption with respect to n_s in the analysis of the spectra, improved fitting is obtained. Finally, we report on the change of the modulation mechanism when n_s crosses from a low to a high electron density regime where phase-space filling modulation dominates.

II. EXPERIMENT

A. Multilayer structure and experimental setup

The structure of the HEMTs, which were grown by molecular-beam epitaxy, is shown schematically in Fig. 1. The indium composition was $x=0.6$ and 0.65 for the strained and $x=0.53$ for the lattice-matched samples. The channel width L_w had values between 10 and 100 nm. For all samples presented below, the *n*-type doping in both donor and contact layers was 4×10^{18} cm^{-3}. However, because of various x and L_w values and, primarily as a result of different spacer widths L_s, the electron density in the channel was dissimilar for each one of the samples investigated. Prior to Hall and optical measurements, the top contact layer was removed by wet etching. The changes $\Delta T/T$ in the transmittivity, induced by modulated He–Ne laser light ($\sim$1 mW) were detected by using a liquid-nitrogen $(LN)_2$-cooled InSb photodiode and analyzed by standard lock-in techniques. Details of the experimental arrangement are given elsewhere.[11]

[a]Present address: University of Maryland at College Park, Department of Materials & Nuclear Engineering, College Park, MD 20742-2115; Electronic mail: dimoulas@eng.und.edu

 0021-8979/96/80(6)/3484/4/$10.00

10 nm	$In_{0.53}Ga_{0.47}As$	contact	n-type 4×10^{18} cm^{-3}
10 nm	$In_{0.52}Al_{0.48}As$		undoped
20 nm	$In_{0.52}Al_{0.48}As$	donor	n-type 4×10^{18} cm^{-3}
L_s	$In_{0.52}Al_{0.48}As$	spacer	undoped
L_w	$In_xGa_{1-x}As$	channel	undoped
1 μm	$In_{0.52}Al_{0.48}As$	buffer	undoped
	InP (100) substrate		

FIG. 1. Schematic of the high-electron-mobility transistor (HEMT) structure. L_w and L_s denote the width of the channel and spacer layer, respectively. L_w values were in the range between 10 and 100 nm.

B. Description of the phototransmittance spectra

The phototransmittance spectra of the samples investigated are shown in Figs. 2(a) and 2(b). The spectral position of each one of the optical transitions depends on many parameters including x, L_w, n_s, and strain. The heavy-hole–light-hole (hh–lh) energy splitting ΔE seen in Fig. 2(a) is a combined effect of strain and quantum confinement. The latter contributes to the splitting by an amount $\Delta E_{qc}=20$ meV (as measured from the lattice-matched sample 682), which is the same for every x value since all samples have the same L_w and similar electron densities. The increase in splitting with x is a result of increased compressive strain due to lattice mismatch $\Delta\alpha/\alpha$ equal to 4.7×10^{-3} ($x=0.6$) and 8.2×10^{-3} ($x=0.65$). By assuming coherent strain[11] with values $\epsilon\simeq-(\Delta\alpha/\alpha)$, the contribution to the splitting $\Delta E_{str}=2b(1+2C_{12}/C_{11})\epsilon$ is estimated to be 33 and 57 meV for $x=0.6$ and $x=0.65$, respectively. The total energy splitting $\Delta E=\Delta E_{qc}+\Delta E_{str}$ is expected to be 53 meV for $x=0.6$ and 77 meV for $x=0.65$. These values coincide with the measured ones from the spectra of samples 694 and 683, respectively. In conclusion, the hh–lh splittings indicate coherently strained heterostructures, free of misfit dislocations.

The lower-energy peaks appearing in the spectra of Fig. 2 are assigned to the ground-state 11*h* optical transition for all but sample 790. In this sample, the ground-state transition is quenched as a result of conduction-band filling effects originating from the high electron density present in the structure. Thus, peak A [Fig. 2 (b)] is assigned to the first 21*h* excited transition, based on the observation that the latter is comparable in intensity to transitions associated with the $n=2$ level in all the other samples. The fact that peak A is much weaker in intensity compared to the 11*h* signal in the other samples in Fig. 2 indicates that A is not associated with the ground-state transition. This is further supported by the fact that if it were related to the 11*h* transition, it would have appeared at energies lower than those of the corresponding peaks in samples 681 and 695 [Fig. 2(b)], based on the values of x, L_w, and n_s.

With the exception of sample 790, the excited transitions indicated by light arrows in Figs. 2(a) and 2(b)] from all other samples exhibit an excitonic character with positive

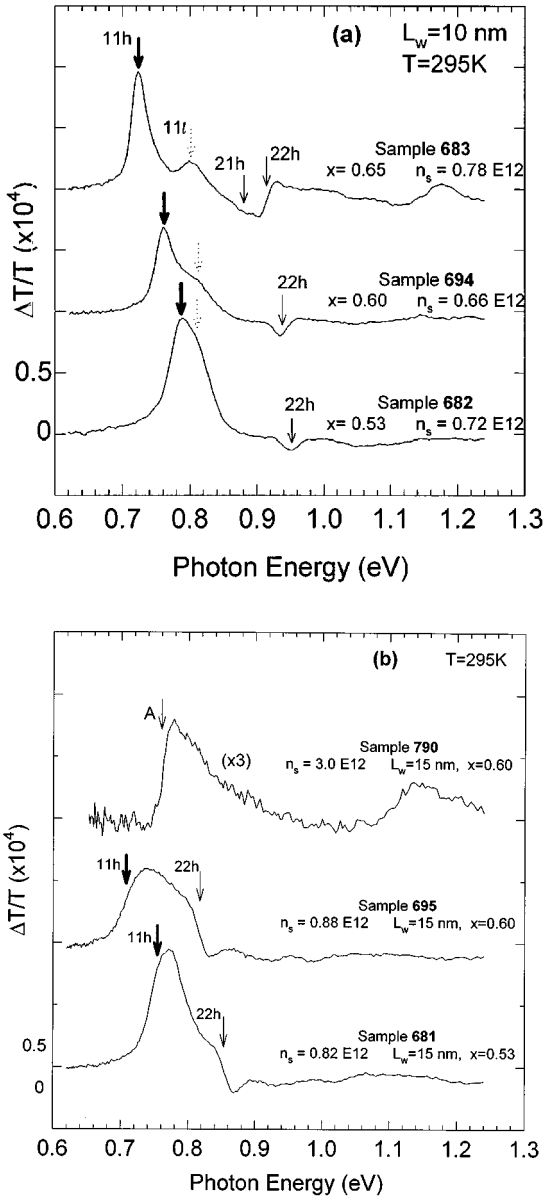

FIG. 2. Phototransmittance spectra of several HEMT structures. L_w and x are the well width and indium concentration, respectively. The quoted values of electron density n_s were obtained by Hall measurements. (a) Samples with the same values of L_w and relatively low electron densities are shown in order of increasing x. (b) Higher-density samples are shown in order of increasing n_s. The bold and light arrows mark the spectral position of the heavy-hole ground and first excited transitions, respectively. The broken arrows mark the spectral position of the light hole transitions.

and negative lobes. On the contrary, the ground-state transition 11*h* has only one positive lobe and is broad and asymmetric with a high-energy tail. These characteristics, which are indicative of exciton screening by the high-density electron gas,[2–5] become more pronounced as n_s increases [Fig. 2 (b)]. The details of the lineshapes contain information about the position of the Fermi level[2–5] relative to the bottom of the conduction subband associated with the optical transition under investigation. This may be used to estimate the electron population in the subband, as discussed in the following section.

III. RESULTS AND DISCUSSION

A. The model

The spectra were analyzed according to the formula $\Delta T/T \simeq -L\,\delta\alpha$, where the absorption coefficient $\alpha \simeq \alpha_0(1-f_e)$.[4,9] Here, α_0 has the form of a broadened step function and represents the absorption coefficient in the undoped case, described by a two-dimensional joint density of states.[4] For the doped case, however, the absorption coefficient α must account for the effects of a degenerate electron gas primarily through the Fermi filling factor[2,4]

$$f_e(n_s) = (\exp\{\beta[\lambda_e(\hbar\omega - E) - \mu_e(n_s)]\} + 1)^{-1}.$$

Here, $\hbar\omega$ is the photon energy, E is the transition energy, $\mu_e(n_s)$ is the chemical potential, $\beta = 1/k_bT$, and λ_e is a function of the effective electron and heavy-hole masses.[2,4] The changes $\delta\alpha$ in the absorption coefficient can be approximated by first-order perturbation analysis as follows:[5]

$$\delta\alpha = \left(\frac{\partial\alpha}{\partial E}\right)\delta E + \left(\frac{\partial\alpha}{\partial\Gamma}\right)\delta\Gamma + \left(\frac{\partial\alpha}{\partial I}\right)\delta I + \left(\frac{\partial\alpha}{\partial n_s}\right)\delta n_s . \qquad (1)$$

The transition energy E, broadening parameter Γ, intensity I, and chemical potential $\mu_e(n_s)$ (measured from the bottom of the corresponding subband level) are used as fitting parameters. The method of nonlinear-least-squares fitting was used to optimize fitting of the spectra. The last term in Eq. (1) mainly describes the effects of directly modulating the phase-space filling by changing the number of electrons in the well,

$$\frac{\partial\alpha}{\partial n_s} \simeq -\alpha_0\left(\frac{\partial f_e}{\partial n_s}\right). \qquad (2)$$

Analytical expressions for α, $\Delta T/T$, and their derivatives with respect to n_s have been given elsewhere.[4] It is worth noticing here that the dependence of f_e on n_s is through μ_e and E; however, the latter quantity decreases slowly ($\sim -n_s^{1/3}$) with increasing n_s due to the band-gap renormalization effect.[12] The latter effect results in a negative contribution with respect to the baseline in $\Delta T/T$, which cannot describe the observed line shapes of the lowest-energy-lying transitions in Fig. 1. On the contrary, μ_e increases with n_s resulting in a positive contribution, which suggests that a direct modulation of the chemical potential by the photogenerated carriers may partly account for the observed line shapes.

The electron density is extracted from the value of μ_e by using a formula[4,12] valid for the case of a two-dimensional electron gas. In general, both levels $n=1$ and $n=2$ are populated at room temperature, with densities $n_s^{(1)}$ and $n_s^{(2)}$, respectively. If the chemical potential relative to the bottom of either one of the subbands is known from the fitting, then the densities can be estimated, provided that the optical transitions are both resolved so that $E_2 - E_1$ is also known.

B. Fitting results and discussion

The fitting curves are compared with the experimental lineshapes in Fig. 3 for two of the samples investigated. In the case of the low-density sample 683, it was found that the first three terms in Eq. (1) give the dominant contribution to the $11h$ line shape. The slight asymmetry on the high-energy side of the peak is an effect of the ''nonoccupancy'' factor $1-f_e$, which also determines the value of the chemical potential. According to the fitting results, μ is positioned 42 meV above E_1 and about 148 meV below E_2 [considering that $E_2 - E_1 \simeq 190$ meV as seen in Fig. 2(a)]. Therefore, almost all electrons occupy only the $n=1$ subband with a density $n_s \simeq n_s^{(1)} \simeq 0.79\times 10^{12}$ cm^{-2}. This agrees well with the value of 0.78×10^{12} cm^{-2} obtained by Hall measurements.

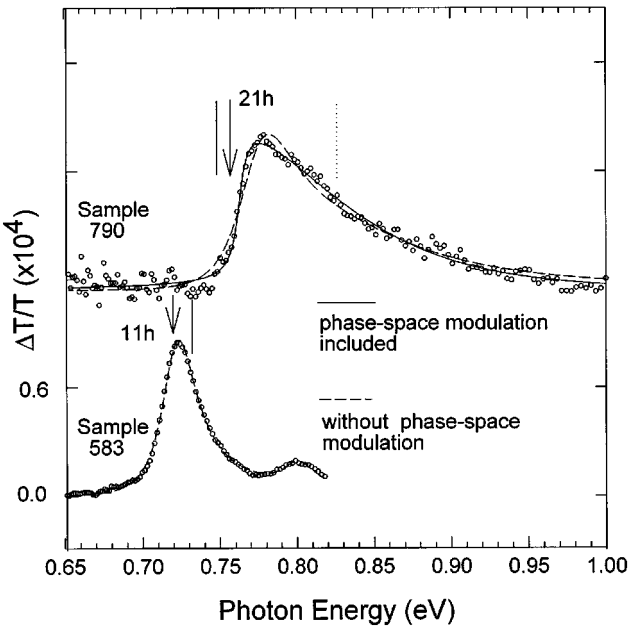

FIG. 3. Comparison of the fitting curves with the experimental line shapes for samples 683 and 790. The experimental points are represented by circles. The solid lines are the fitting curves obtained when the modulation of phase space is included. The dashed line in sample 790 represents the fitting results without the phase-space modulation. The solid vertical lines mark the position of the chemical potential as determined by the fitting while the dotted vertical line marks the position of the chemical potential when phase-space modulation is not included.

The higher-density sample 790 (Fig. 3) exhibits a distinctly different line shape at the $21h$ transition with a more pronounced asymmetry compared to the low-density sample 683. The dashed line in Fig. 3 is the fitting curve obtained by considering only the first three terms in Eq. (1). This model fails to describe the steep rise at the onset of the transition. Besides, it predicts a value $\mu - E_2 \simeq +60$ meV, which is much higher than expected on the basis of Hall measurements.

The inclusion of the term $-\alpha_0(\partial f_e/\partial n_s)$ in the sum of Eq. (1) improves considerably the fitting for sample 790, as shown by the solid curve in Fig. 3. Moreover, this term dominates the line shape suggesting that, in this high-density sample, the phase-space filling modulation mechanism is dominant as a result of the laser-induced modulation of the electron concentration in the well. According to the model, μ is positioned 10 meV below the $n=2$ level implying a density $n_s^{(2)} \simeq 0.2\times 10^{12}$ cm^{-2} of electrons filling the second electron subband. The total density n_s in the channel was

estimated to be 2.0×10^{12} cm^{-2}, substantially smaller than the $n_s\simeq3.0\times10^{12}$ cm^{-2} obtained by Hall measurements. This discrepancy may be explained by inaccuracies in determining the subband energy separation E_2-E_1 due to the unresolved 11*h* transition in sample 790. To estimate the total density in this sample, E_2-E_1 was taken to be about 90 meV, which is the value of subband separation measured in samples 681 and 695 [Fig. 2(b)]. This was based on the assumption that the samples 790, 681, and 695 have the same subband structure since they all have the same channel thickness L_w. However, the formation of a triangular potential well at the heterointerface due to high electron density in sample 790 may significantly alter the subband structure resulting in a lower estimate of n_s by phototransmittance. It is worth noticing that the 11*h* transition in heavily doped HEMT structures is clearly observed in low-temperature photoluminescence spectroscopy,[13] although the first excited transition is weak and, in most of the cases, it is not resolved.[13] Therefore, modulation spectroscopy, combined with photoluminescence, could yield the total electron density as well as the electron population in each one of the subbands, resulting in a complete noninvasive characterization of HEMTs with respect to n_s.

Several other samples shown in Figs. 2(a) and 2(b) were also analyzed using the model of Eq. (1). In sample 694, μ is only within 1 meV from the bottom of the $n=1$ subband resulting in a total density of $n_s\simeq n_s^{(1)}\simeq0.3\times10^{12}$ cm^{-2}, only half the value obtained by Hall measurements. The less successful fit and the discrepancy in the measured values of n_s are due to the interference of the lh signal with the high-energy tail of the hh peak. In the lattice-matched samples [sample 682 in Fig. 2 (a) and sample 681 in Fig. 2 (b)] where hh and lh merge, it was not possible to find a unique fitting solution with acceptable parameter values.

IV. CONCLUSIONS

Electron density effects in $In_xGa_{1-x}As/\ In_{0.52}Al_{0.48}As/$ InP HEMT structures can be studied by phototransmittance at room temperature. For low electron density and large compressive strain ($x=0.65$), where light- and heavy-hole transitions are well separated spectrally, stable fitting results were obtained, in agreement with Hall data. In lattice-matched samples, the analysis of the spectra is hampered by the merging of light- and heavy-hole transitions. In high electron density (above 2.0×10^{12} cm^{-2}) samples, the determination of the density of electrons occupying the second electron subband is possible by analyzing the first excited transition. However, an estimate of the total electron density in the channel is less accurate mainly due to the lack of information about the spectral position of the ground state optical transition in high-density channels. Nevertheless, phototransmittance may complement either photoluminescence or Hall measurements in which case both a separate estimate of the electron densities in the two subbands as well as an accurate estimate of the total density in the channel are possible, thus providing a complete characterization of HEMTs. Finally, by including the modulation of the phase-space filling as a result of changes in the electron concentration in the channel, the model improves characterization with respect to the electron density. This is particularly important for the case of high electron density structures where the latter modulation mechanism dominates the line shape of the spectra.

[1] See a review article by F. H. Pollak and H. Shen, Mater. Sci. Eng. **R10**, 275 (1993), and references therein.
[2] Y. Yin, H. Qiang, F. H. Pollak, D. C. Streit, and M. Wojtowicz, Appl. Phys. Lett. **61**, 1579 (1992).
[3] Y. Yin. H. Qiang, D. Yan, F. H. Pollak, and T. F. Noble, Semicond. Sci. Technol. **8**, 1599 (1993).
[4] A. Dimoulas, K. Zekentes, M. Androulidaki, N. Kornelios, C. Michelakis, and Z. Hatzopoulos, Appl. Phys. Lett. **63**, 1417 (1993).
[5] A. Dimoulas, K. Zekentes, and M. Androulidaki, Mater. Res. Soc. Symp. Proc. **324**, 205 (1994).
[6] G. Gumbs, D. Huang, Y. Yin, H. Qiang, D. Yan, F. H. Pollak, and T. F. Noble, Phys. Rev. B **48**, 18 328 (1993).
[7] E. S. Snow, O. J. Glembocki, and B. V. Shanabrook, Phys. Rev. B **38**, 12 483 (1988).
[8] Y. S. Tang, J. Appl. Phys. **71**, 2392 (1992).
[9] I. Bar Joseph, J. M. Kuo, C. Klingshirn, G. Livescu, T. Y. Chang, D. A. B. Miller, and D. S. Chemla, Phys. Rev. Lett. **59**, 1357 (1987).
[10] L. D. Nguyen, A. S. Brown, M. A. Thompson, and L. M. Jelloian, IEEE Trans. Electron Devices **ED-39**, 2007 (1992).
[11] A. Dimoulas, J. Leng, K. P. Giapis, A. Georgakilas, C. Michelakis, and A. Christou, Phys. Rev. B **47**, 7198 (1993).
[12] See for example, R. Cingolani and K. Ploog, Adv. Phys. **40**, 535 (1991).
[13] A. Tabata, T. Benyattou, G. Guillot, A. Georgakilas, K. Zekentes, and G. Halkias, Appl. Surf. Sci. **63**, 182 (1993).